Journal of Mines, Metals and Fuels, *71(12C) : 265-275; 2023. DOI: 10.18311/jmmf/2023/47308*

Print ISSN : 0022-2755

Journal of Mines, Metals and Fuels

Contents available at: *www.informaticsjournals.com/index.php/jmmf*

A Thorough Analysis of the Chemical and Physical Characteristics of Metal Oxide Coated Fly Ash Cenospheres: Waste Generation in Thermal Power Plants and their Photocatalytic Research

H. N. Hema[1,2,3] and Murali Krishna Panchangam[2,3*]

[1]Department of Chemistry, M.E.S Kishore Kendra P U College, Malleswaram, Bengaluru – 560003, Karnataka India
[2]Department of Chemistry, Ramaiah Institute of Technology, Bengaluru – 560054, Karnataka India; muralikp@msrit.edu
[3]Visvesvaraya Technological University, Belagavi – 590018, Karnataka India

Abstract

Several nanocomposites prepared from a coating of metal/metal oxide nanoparticles on Cenospheres have a special property. The primary nanoparticles are closely stacked together without interparticle voids and formed on the cenosphere shell, providing a high surface area for the photocatalytic degradation of dyes. These numerous nanocomposites were characterised by various techniques such as Field emission electron scanning microscopy, energy dispersive X-ray, X-ray diffraction, Fourier Transformation Infrared, Ultraviolet-Visible spectroscopy, Scanning Electron Microscopy and Transmission Electron Microscopy. The mesoporous structure of all the nanoparticles and the strong adsorption ability of activated fly ash cenosphere accounted for the notable degradation performance.

Keywords: *Cenospheres, Nanocomposites, Photocatalytic Studies*

1.0 Introduction

Electricity is produced all over the world using coal. Thermal power plants that burn coal currently supply around 41% of the world's electricity, and that number is predicted to rise to about 44% by 2030[1]. By burning coal huge volumes of fly ash are obtained. Global production is about 750 million tonnes per year, and it is increasing. Due to the relative cost of waste, various value-added applications have been proposed. The utilisation of fly ash is only about 25% of weight all over the world, 10% of weight in Australia, 15% of weight in Russia, 39% of weight in the US, 47% of weight in Europe and 68% of weight in China. Nevertheless, Figure 1 highlights numerous possibilities for its re-use. This indicates that there are still sizable volumes, which are currently used in filling lands[2]. The component of fly ash which is the Cenosphere is important in preparing more useful products from it. Because of their unique properties, such as being inert towards chemicals, less water absorption, low density, nontoxic, high insulation, non-metallic which is good thermal resistant, hollow microparticles and are light in weight with high compressive strength. They are excellent for various industrial applications because of these characteristics[3]. As a result, this review will concentrate on cenospheres and describe their creation, characterizations, methods of separation, and prospective applications.

**Author for correspondence*

1.1 The Cenosphere

The cenosphere has a density of less than 1gm/cm and is called "Cenospheric" and floats on water therefore it is probably termed a Cenosphere. It has a size ranging between 1 to 500 microns with an average compressive strength of up to 7000⁺ psi.

1.2 Characterization of Cenosphere

Some of the physical characteristics, like the thickness of the shell, the size of the particle and also the distribution of particle size and shell thickness, play a significant role in the performance of the lightweight composites' cenosphere[4,5]. For example, when the final application requires the strength of cenosphere composites, the thickness of the cenosphere particles plays a critical role. This is because thick shell particles provide higher strength compared to thinner shells. Since spherical shapes have the lowest surface area to volume ratios, wetting the surface with resin, binder, and water requires the least amount of these materials. This is why it is important to consider surface morphology rather than shell thickness. The burning of coal and its parent material produces the chemical makeup of cenospheres[6,7]. The main ingredient is cenospheric aluminosilicate, with minor amounts of essential metals like Mg, Fe, K, and Ca as well as trace amounts of Na, Ti, S, and P.

1.3 Phase Composition

Cenospheres are mostly composed of Si and Al, with the least metals like Ca, K, Fe, Na, Ti, and Mg. All of these metals are mixed in crystalline and amorphous phases rather than being present in their pure oxide forms. Mullite, cristobalite-quartz, K-feldspars, acid plagioclases, and magnetite are the different crystalline phases. Cenospheres are infused with quartz, lime, and periclase apart from these. The cenosphere particles' skeleton is made up of these clusters of crystalline phases. This skeleton structure, which has a pattern resembling needles, gives cenospheres structural stability across a wide temperature range[8,9]. About 90% of an amorphous glass phase, which offers a smooth surface, surrounds the skeleton of cenospheres. A flat surface is made available because this layer is made up of glass[10,11]. The layer of glass in the cenosphere easily reacts with HF and gets removed. The two primary phases of the cenosphere are calcite, Gypsum, dolomite and portlandite are just a few minor phases that could show up on the shell's surface depending on how the material is separated, dried, and stored. These forms are mostly the product of the dissolution of fly ash's lime, periclase, and gypsum-anhydrite in the wet separation process. Brucite, Gypsum and portlandite can change into more stable forms like carbonates, such as magnesite, calcite and dolomite, and when cenospheres are dried by collecting carbon dioxide from the atmosphere. Figure 2 shows a schematic representation of cenospheres.

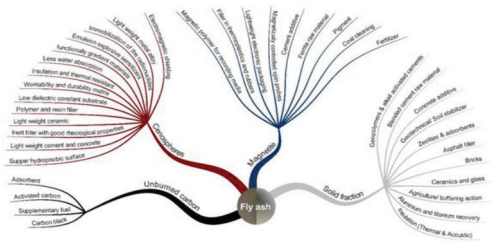


Figure 1. Commercial uses of several varieties of fly ash[2].

2.0 Textile Dye Pollution

Water pollution brought on by textile dye emissions is still a global environmental problem. These untreated textile effluents include various chemicals, several colours, and organic and inorganic compounds that contain trace metals like Cr, As, Zn and Cu. These elements are harmful to the ecology[12]. Over 100,000 different varieties of commercially accessible dyes exist in total, and Ninety percent of them are predicted to be used in textiles. The chemical, paper, leather, and plastic industries provide the remaining 10%. These dye-contaminated effluents are released into the natural water, due to the constant use of these dyes and releasing less than a part per million in water causes aesthetic issues and has contributed to the light reaction which takes place in water plants. These unwilling to cooperate with the environmental dyes which are toxic cause carcinogenic,

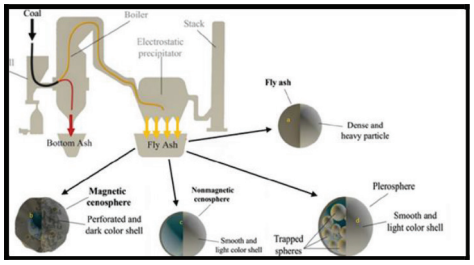


Figure 2. Schematic of (a) heavy particles (solid form), (b) formation of magnetic cenospheres, (c) formation of magnetic cenospheres which are non magnetic, (d) plerospheres[2].

genotoxic, teratogenic and mutagenic to flora and fauna and also to human health in long-term exposure[13].

3.0 Photocatalysis

Greek is the language from which this word originated. It becomes the terms "photo" (phos) and "catalysis," which are separated apart (katalyo). The prefix "phos" in English means brilliance, whereas "katalyo" means separation or breakdown.

But all you have to do is designate it as a photoreaction. that is accelerated when a catalyst is present. Photocatalysis is defined as "a change in the pace of a chemical reaction by the presence of a photocatalyst via regeneration of electron-hole pairs accompanied by the absorption of photon energy under the exposure to UV or visible light" in a valid scientific definition.

Basic Mechanism of Photocatalysis:

(a) Photoexcitation:

$$TiO_2 + h\nu \xrightarrow{h\nu \geq E_{BG}} h^+_{VB} + e^-_{CB}$$

(b) Ionization of water:

$$H_2O \rightarrow OH^- + H^+$$

(c) Oxidation and reduction:

$$(O_2)_{ads} + e^-_{CB} \rightarrow O_2^{\bullet -}$$

$$H_2O + h^+_{VB} \rightarrow OH^{\bullet} + H^+$$

(d) Protonation of superoxide:

$$O_2^{\bullet -} + H^+ \rightarrow HOO^{\bullet}$$

(e) Recombination of electron-hole pairs:

$$HOO^{\bullet} + e^-_{CB} \rightarrow HO_2^-$$

$$HOO^{\bullet} + h^+_{VB} \rightarrow H_2O_2$$

4.0 Photocatalyst

4.1 Some Photocatalysts that are Semiconductor-based

Most photocatalysts consist of semiconductor which is chemically stable and photosensitive, electronic structure of metal atoms which has filled VB, and empty CB. Here are some of the criteria, like irradiation wavelengths of light, band gap energy and adsorption of pollutants required by a good photocatalytic property of metal oxide. Larger bandgap metal oxides can only be activated in the ultraviolet, but smaller bandgap metal oxides can be more effective in photocatalysis in the visible light spectrum[14]. The n-type semiconductor Zinc Oxide (ZnO), has a 3.2eV band gap which is slightly wide and this n-type semiconductor has a massive exciton of 60meV binding energy. The utilization of the binding energy of 60meV has received a lot of attention from researchers. Owing to its distinct feature, it finds application in the fields of solar cells, sensors, electrodes, transducers, and even photocatalysts. Some of its notable attributes include robust pyroelectric characteristics, strong luminescence at room temperature, strong electron mobility, and excellent transparency to visible light. ZnO has three possible crystalline forms: rock salt, zinc blend and wurtzite. Among these rock salt ZnO and Zinc blende are rare to synthesize, but wurtzite, a hexagonal crystal structure is easily synthesized in a short period and usually under various conditions they are stable. Because of this thermodynamic stability, ZnO is considered to be a good photocatalyst.

The transition metal oxide ZnO has a single, broad, strong adsorption band and has an electronic configuration of $[Ar]3d^{10}4s^0$. Photoluminescence (PL) spectra were utilized to examine the luminescence features of ZnO. These spectra demonstrate that ZnO flaws and other impurities cause broad visible emission (about 510 ± 580 nm) as well as strong UV emission (386 nm). Consequently, ZnO can absorb more solar spectrum than other semiconducting metal oxides. Due to some effects like the quantum size effect and surface effect of ZnO which are nanostructured ZnO has become an attractive choice in green photocatalytic systems. It has been thoroughly studied and manufactured utilizing several synthesis methods in a range of nanosheets, nanoflowers, nanorods, nanowires, nanocombs, growth morphologies and nanoparticles[15]. To enhance the reaction activity of ZnO photocatalyst, it is doped with oxides of other metals like V_2O_5, Mn_2O_3, CuO, CeO_2, CdO, Mn_2O_3, metals like Ag and polymer[16,17].

Based on ZnO nanoparticles' characteristic features, like n-type conductor, negative conductivity and large band gap of SnO_2 metal oxide which is amphoteric and colourless has been chosen for photocatalytic activity. Since

SnO_2 has a bandgap energy of 3.60 eV, It is a material that shows promise for use in many applications, including gas sensors, liquid crystal displays, solar cells, optoelectronic devices, infrared-red reflectors, and raw materials for transparent films[18]. SnO_2 is a good photocatalyst because of its high electrical conductivity, chemical resistance, thermal stability, and affinity towards CO and H_2 and also has great reflectivity in the infrared region[19,20]. In a SnO_2 unit structure, coordination of (6, 3) is mainly because Six oxygen ions engulf the tin(IV) ion, and three tin(IV) ions surround that oxygen[21]. The high annealing temperature of Sn creates a vacancy by crystallization, and SnO_2 has great thermal stability which helps in increasing the lattice space of SnO_2 crystal. The crystalline structure of SnO_2 will change as the annealing temperature is increased. In asymmetric rutile, the Sn-O octahedron rises in agreement. This is highly beneficial for SnO_2 to retain its crystallinity which results in a bigger surface area, for its photocatalytic application. To hold more reactants during adsorption. Hence SnO_2 is proven to be a good photocatalyst[22].

Bi_2O_3 has chosen to be a good photocatalyst as it possesses a wide Bandgap (range from 2.00 to 3.96eV) and also a few characteristics properties like high refractive index, high di-electric permittivity and marked photoconductivity as well as photoluminescence[23]. Bi_2O_3 has crystalline forms α, β, γ, δ, and ω-Bi_2O_3. These characteristic features of Bi_2O_3 are applicable in various fields like sensor technology, and optical coatings, and are used to prepare electrochromic materials. $BiVO_4$ which has a band gap of 2.40eV and an absorption of solar spectrum fraction up to blue light of Ca.520 nm, is good and strong in degrading organic pollutants, under visible light, it undergoes water splitting. Hence $BiVO_4$ proves itself to be a good photocatalyst. A combination of $BiVO_4$ along Bi_2O_3 proves to be an excellent photocatalyst because of having higher absorption in the visible light region spectra, as it is also considered to be more effective and practical than TiO_2 [24].

Table 1. Band gaps and energy levels of metal oxides (semiconducting)

Metal oxide	Eg (eV)	E_{CB} (eV)	E_{VB} (eV)
ZrO_2	5.00	-3.41	-8.41
Ga_2O_3	4.80	-2.95	-7.75
NiO	3.50	-4.00	-7.50
SnO_2	3.50	-4.50	-8.00
Nb_2O_5	3.40	- 3.40	-6.80
TiO_2	3.20	-4.21	-7.41
ZnO	3.20	- 4.19	-7.39
In_2O_3	2.80	-3.88	-6.68
WO_3	2.70	-5.24	-7.94
Fe_2O_3	2.20	-4.78	-6.98
CuO	1.70	-4.96	-6.66

Based on the band gap and irradiation light needed metal oxides are classified into 3 types

i. Those Metal oxides with a band gap above TiO_2 behave to a better photodegradation rate under UV light, mainly used to degrade organic pollutants.
ii. Metal oxides with a band gap equal to TiO_2 behave as a better photodegradation requiring UV light.
iii. When exposed to visible light, the majority of metal oxides with band gaps lower than TiO_2 exhibit better photodegradation rates.

Table 1 lists the energy levels and band gaps of semiconducting metal oxides[25]. the determined valence band (E_{CB}) and conduction band (E_{CB}) in electron Volts are

For example, like WO_3, CeO_2 also showed a better degradation than TiO_2 under visible light for degradation of organic pollutants though they have a smaller bandgap of 2.94eV

TiO_2 anatase shows the highest photocatalytic degradation among those semiconductors which have a bandgap of 3.00eV under UV light irradiation.

ZrO_2 (E_g=5.00eV) showed 2 times higher photocatalytic activity than TiO_2 under UV irradiation for degradation of RhB[26].

NiO (E_g =3.7eV) also proved to be an efficient photocatalyst than TiO_2 in the degradation of phenol using water.

Ga_2O_3 (E_g =4.8eV) can only be used in reductive photocatalytic reactions with UV light irradiation[27].

In_2O_3, Fe_2O_3, SnO_2, V_2O_5, Cr_2O_3, CuO, and MoO_3, (all these metal oxides are used for photocatalytic oxidation under UV light irradiations.

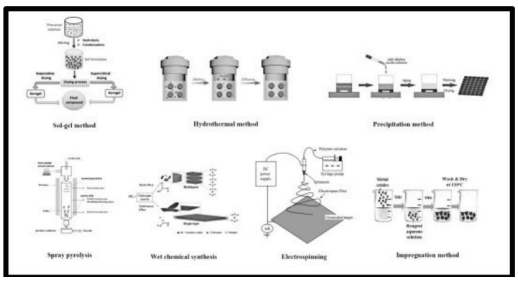


Figure 3. Schematic representation of different methods of preparation[28].

Table 2. Preparation techniques of ash-based nanocomposites[28]

Methods of preparation	Photocatalyst produced from ash	Outcome
Sol-gel	AgCl-TiO_2/FACs	obtained by mixing $AgNO_3$ solution with titanium solution later by dissolving in FACs, and maintain 70^{0}C to vacuum dry
Sol-gel	Fe^{3+}-TiO_2/FACs	FACs that have been acid-treated are synthesized by adding them to a titanium sol that contains polyethylene glycol (PEG) and $Fe((NO_3)_3 \cdot 9H_2O)$, along with aging the mixture for 24 hours, and then filtering, drying, and calcining it for two hours at 450 ^{0}C.
Sol-gel	Fe-N-TiO_2/FACs-Cts	FACs-Cts that have been acid-treated are combined with an active solution TBOT (18 ml), C_2H_5OH (50 ml), PEG-400 (10 ml), $Fe(NO_3)_3 \cdot 9H_2O$ and urea is added. This mixture is then ultrasonicated for one hour, allowed to age for twenty-four hours, dried, and then calcined at 823 K for two hours while under N_2 flow.
Modified metalorganic decomposition (MOD)	$BiVO_4$/FACs	prepared by combining the active solution ($Bi(NO_3)_5 \cdot 5H_2O$ and acetic acid) with the tri-isopropoxy oxide of vanadium(V) and acetylacetone for one hour while adding FACs. This was followed by calcination and drying in air at 500°C for two hours, and evaporation at 80°C.
Pyrolysis	CeO_2/FACs	made by mixing the active solution ($Ce(NO_3)_3 \cdot 6H_2O$, ethanol, and distilled water) with propylene oxide, acetylacetonate, and NH_4OH dropwise till pH 6. Then, FAC is added, and the mixture is chilled overnight, evaporated, dried, and calcined for an hour at 450 °C.

Fe_2O_3 and V_2O_5 are not photocatalysis under water as **Fe** and **V** oxides undergo corrosion.

5.0 Photocatalytic Nanocomposites which are Ash-Based

5.1 Methods of Preparation

Utilizing volcanic ash, coal fly ash, and rice husk ash as catalytic supports is actively being researched. Different preparation methods(Figure 3) that could be used to degrade the type of pollutant, catalyst, support, and in-situ hydrolysis include hydrothermal decomposition, Sol-Gel, precipitation, hydrothermal, co-precipitation, hydrolysis precipitation, pyrolysis, modified Metal-Organic Decomposition (MOD), wet chemical synthesis, solvothermal, impregnation, Layer-By-Layer Assembly (LBLA), polycondensation, electrospinning, ion exchange, impregnation, in-situ hydrolysis, and polycondensation.

Table 2 provides a thorough summary of the preparation techniques for the ash-based nanocomposites.

6.0 Investigation

6.1 Study by SEM Images

We discuss SEM images(Figure 4) of several FAC-supported photocatalytic composite types. Various metal oxides including TiO_2, $BiVO_4$, and CeO_2, are coated on the cenosphere and did not noticeably disrupt the morphological structure of FACs. These instances involved generally homogenous metal oxide layers on the surface of FACs with some metal oxides completely covered here and there, which causes the surface to be rough and contain pores and cracks. However, the ZnO-doped cenosphere composite had a different surface morphology than other metal oxide cenosphere. Only ZnO-coated cenosphere showed the coating almost like a flower in a group of varying sizes[29]. Existing morphological modifications are mostly the result of the development of ZnO flowers that spread throughout the FAC matrix and took the shape of clusters. Since the majority of the catalytic reaction occurs on the catalyst's surface, it is well-known that surface features are important for assessing a catalyst's photocatalytic efficacy. According to the results, when creating ash-based nanocomposite, the uneven morphological contour of FACs porosity showed how well-available a particular spot and a surface binding site were designated for photocatalyst deposition[30]. Furthermore, the surface-to-volume ratio of the ash-based nanocomposite increases due to its decreased overall size. This property improves the efficient degradation of dye pollutants within the FAC matrix by promoting the synergistic adsorption from the ash support and the photocatalytic activity from the photocatalyst. It surely provides a more catalytic and

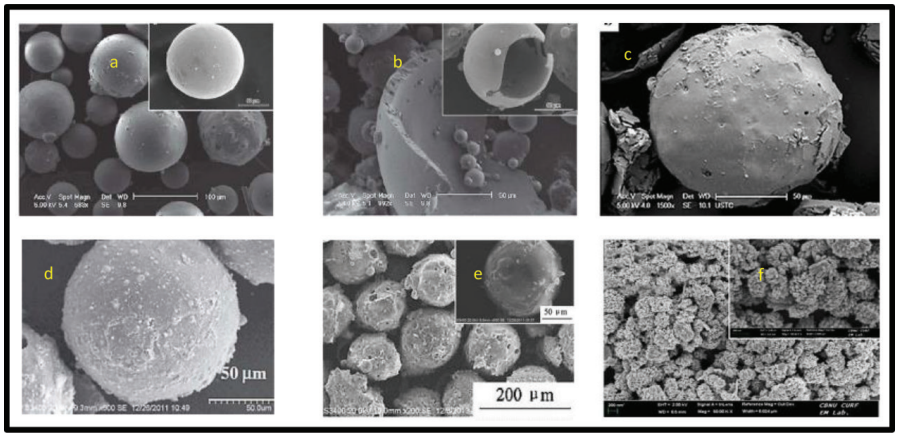


Figure 4. Images of SEM (a) raw, (b) broken FACs, (c) TiO_2-FACs, (d) $BiVO_4$-FACs, (e) CeO_2-FACs, (f) ZnO-FACs[28].

adsorptive surface-active site, hence generating a higher generation of hydroxyl radicals linked to the acquisition of photons that are greater than activation energy[31,32].

6.2 X-ray Diffraction Study

The presence of All diffraction peaks obtained in TiO_2-FACs, which are attributed to the quartz Q (SiO_2) and mullite M ($3Al_2O_32SiO_3$) including at 2θ=24° there is a broad peak, some points occur due to the amorphous phase of aluminosilicate in FACs and FAC-based composites (Figure 5)[33]. At approximately 25.3° at 2θ, there are peaks due to TiO_2 in the anatase phase which implies the (101) diffraction planes, based on JCPDS Cards No. 21-1272[34]. In the XRA patterns of TiO_2-FACs, we can also find a characteristic peak due to anatase TiO_2 which clearly shows the perfect coating of metal oxide TiO_2 on Fly Ash Cenospheres. This result suggests that the metastable crystalline structure of the photocatalyst may be preserved during the anatase TiO_2 immobilization process onto the fly ash substrate[35].

6.3 Fourier Transform Infrared Spectroscopic Studies

An important tool is the Fourier transform infrared study helps in the characterization of the present surface functional groups on the surface, which is essential for the adsorption and degradation of dye contaminants. Figure 6 shows the photocatalytic composites FTIR images. In the IR spectrum, a bending peak at the region between 1692 cm^{-1} and 1634 cm^{-1} is observed because when the H_2O is added to the lattice of silica a bending vibration is obtained[38]. In contrast, a stretching in Si-OH to O-H and

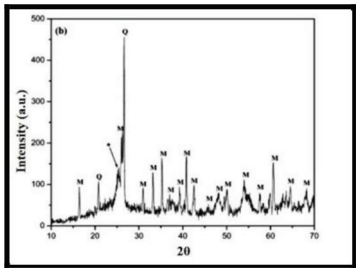


Figure 5. XRD pattern of FACs-based composites[28].

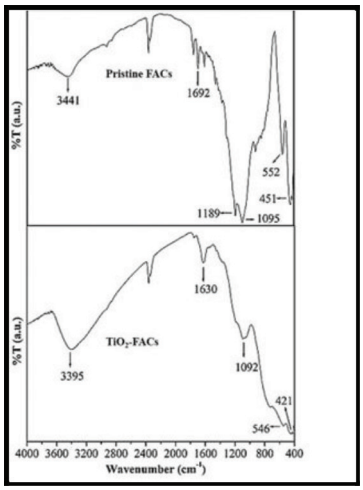


Figure 6. FTIR of FACs-based composites[28].

water molecules adsorption to the surface of the catalyst gives a vibrational peak in the region 3469-3432 cm^{-1} [35]. At 1189 cm^{-1} asymmetric vibration of Al-O-Si is detected, and more spectra at 1095-1074 cm^{-1} Si-O-Si asymmetric stretching. Si-OH bond for stretching vibration is obtained due to transmittances at 966/963 cm^{-1} reported by Ahmed and Adam[36]. Significantly, after the catalyst

Table 3. Photodegradation of dye pollutants[28]

Dye pollutants	Metal oxide coating on cenosphere (Catalyst)	Removal (%)	photocatalyst weight (g)	Concentration of the Solution (mg/L)	Volume of Solution (mL)	Degradation time (minutes) taken by source of light
MB	Fe^{3+}-TiO_2/ FACs	50.0	1.800	20.0	600	- Visible light
MB	N-TiO_2/FACs	58.0	1.800	20.0	600	540 Visible light
MB	$BiVO_4$/FACs	90.0	0.200	10.0	50	300 Visible light
MB	Pt-$BiVO_4$/FACs	93.0	0.200	10.0	50	120 Visible light
MB	CeO_2/FACs	60.0	0.200	10.0	50	300 Visible light
Methyl orange	$BiVO_4$/FACs	82.0	0.200	10.0	50	150 Visible light
Rhodamine B	Fe-N-TiO_2/ FACs-Cts	93.1	0.200	8.0	50	240 Visible light

was coated for FACs, the intensity of the peaks for Si-O-Si and Al-O-Si decreased and finally disappeared, Si-O-Sn, Si-O-Ti, Al-O-Ti, and Si-O-Ti linkages are found between the catalyst and ash, in that order, suggesting the establishment of functional groups. Some more IR bands at 451cm^{-1}, 457 cm^{-1}, 463 cm^{-1}, 471 cm^{-1} and 480 cm^{-1} for Si-O-Si bending vibration is observed[37].

7.0 Investigation of Dye Degradation by Different Photocatalytic Methods

Numerous textile colours were used as the primary model pollutant in the study of the use of the metal oxide-coated cenosphere. The literature states that several operating parameters were also looked at, such as the temperature due to calcination, loading of the catalyst, dye concentration initially, and pH of the solution. Table 3 provides information on the application and operating circumstances for dye removal.

7.1 Effect of Temperature Required for Calcination

The effectiveness of dye pollutant degradation is significantly influenced by the temperature required for calcination. The temperature required for calcination has a significant impact on the TiO_2 ash-based composite which is active photocatalytically because the size and development of TiO_2 crystals are greatly influenced by the reaction temperature needed for the calcination process. The temperature required for calcination is from 350°C to 650°C to obtain N-TiO_2/ FAC nanocomposites. Wei *et al.,* studied the impact of temperature required for calcination which is used in the degradation of MB degradation[38]. It was noted that when the temperature required for calcination rose, both the produced composite's capacity for photocatalysis and the effectiveness of MB's decomposition improved. But as the temperature surpassed 450°C, the rate of disintegration decreased. Wang *et al.*, reported similar results[29]. As the temperature required for calcination rises to 350-450°C, the consequence is confirmed to obtain anatase phase transformation from amorphous TiO_2, and this process helps to strengthen the catalyst's ability to degrade. On the other hand, the production of the crystalline TiO_2 rutile form, which results in bulky growth of the particle size and a wider Band gap, slows the process of dye degradation. when the temperature required for calcination climbs to 650°C[29]. These factors led to the literature's findings that the typical range of temperatures needed for calcination was 300–400°C to obtain TiO_2-coated ash-based nanocomposites.

7.2 Effect on Loading the Catalyst

The primary factor impacting the operation costs and viability for large-scale practical applications is catalyst loading. The effect of catalyst loading on the MB degradation was examined in the study by increasing the catalyst amount from 0.5 g/L to 20 g/L. According to the results, a rise in catalyst loading was observed. This is because the decolourization rate increased. These results were in line with the findings of the study conducted on the degradation of dye MB photocatalytically[39]. This was done by utilizing Pt metal doped on TiO_2 metal oxide which in turn was coated on the cenosphere as nanocomposites. These outcomes are attributed to a higher catalyst loading due to the greater availability of

surface-active sites for the exposure and adsorption of dye molecules. In the meantime, greater the loading of a catalyst may result in a higher absorption of light, which in turn encourages the enhancement of the formation of hydroxyl radicals generated by light and a larger exciton of electrons activated by light, both of which increases the degradation of dye molecules employing photocatalysis[50].

However, Wang, et al investigation's found that as catalyst loading grew over the recommended level, the degrading efficiency of MB remained constant. This result was attributable to the continued overdosage of catalyst slurry, which could lead to excessive catalyst particle agglomeration and parts of the catalyst surface being occluded from photon absorption[44]. Furthermore, the studied solution's transparency may be compromised by the photocatalyst's aggregation, which would also decrease the frequency of photons striking the catalyst surface and lessen light penetration[41]. These barriers may gradually decrease the quantity of photogenerated hydroxyl or superoxide radicals, so significantly slowing the breakdown process[42]. Based on the loading of a catalyst may cause catalyst particles to collide and have a further effect on the catalyst's deactivation. Therefore, the photocatalytic process would be delayed by the lower rate of collision between the photocatalyst and dye pollutants[43].

7.3 Some Results of Initial Dye Dosage Effects

At various beginning concentrations, the change in dye degradation concerning the illuminating period was investigated and found that raising the initial dye concentration typically resulted in less efficient degradation[44]. As more dye compounds were entrapped onto the outer body of the photocatalysts at the higher starting concentrations, this result might be explained by the excess of active sites on the surface and the weaker hydroxyl radicals[45]. The overloaded adsorbed dye molecules would collide or get blocked as the concentration increased, necessitating prolonged contact and several increasing illuminating periods to achieve the gradual breakdown of these dye substances. When the surface binding sites were overwhelmed with pollutants, the created in-between substances obtained from the process of photocatalysis would disperse slowly onto the catalyst surface and destroy the activity of the intermediate products[46].

Similar to this, a higher initial dosage boosts the solution's non-transparency to cause a scattering effect on light. This reduces the amount of light used by the photocatalyst for the photocatalytic activity because of photon activation limit is very low and also during the photodegradation process reactive radical species are formed. species radicals[47]. It's possible that at this point dye molecules undergo photolysis rather than photocatalysis[48]. As a result, an increase in the dosage will slow down the degradation.

7.4 pH Effect on Dye Solution

Dye solutions pH is the key variable which influences some of the factors like surface charge, production of hydroxyl radicals, properties of catalyst surface and ionization of the dye molecules in any basic photocatalytic reaction[49]. When there is a pH change in the dye solution there is a lot of change in water solubility, also displays a wide change in the range of physicochemical three different forms for speciation behaviour like hydrophobicity, and the aqueous solution: neutral, positive, and negative. According to the point of zero charges (pHzpc) theory and pKa value, there is a change in degradation efficiency for the nanocomposite and the pH of the solution has an impact on the dye molecules' acid-base properties[50]. From the perspective of no charges When the catalyst surface clings to the net-zero point of charge, pH equals pHzpc. A pH greater than pHzpc causes the catalyst surface to grip, creating a net negative surface charge. When pH is less than pHzpc, the catalyst surface grips similarly to a net positive surface charge[51].

Anionic dye often had a higher degradation efficiency in acidic solution whereas cationic dye preferred basic conditions. Stating an example of the dye MB, Peng *et al.*, found that lower pH levels resulted in less MB clearance, whereas the effectiveness of the degradation improved as the pH rose from 3-9 [52]. The rate of MB degradation breakdown at the reduced pH. Because both the charged nanocomposites and MB obtain the same kind of positive charge, which repels one another electrostatically. Along with this, there are also H^+ ions in the medium of lower pH competing with the dye MB positive charges to hold the surface binding sites which will also contribute to poor MB removal in the acidic solution[53]. Positively charged MB cations are electrostatically attracted to negatively charged surface active sites at higher pH levels, It improves the efficiency of degradation and greatly

increases the adsorptive absorption of the molecules of the dye MB. Additionally, more hydroxyl ions are available in the initial state, and these ions will react with holes to produce additional hydroxyl radicals. Consequently, the photocatalytic efficacy of MB increases with rising pH levels. However, when the pH rises above 11, the removal of MB decreases because the catalyst surface is saturated due to the entire adsorption of hydroxyl ions over the dye molecules.

7.5 Light Source Effect on the Dye Solution

The photocatalytic composites' bandgap and the light sources affect how quickly a photocatalytic process degrades[53]. There is no doubt that a photocatalytic composite with a broad bandgap performs better when exposed to UV radiation. Whereas, those photocatalyst composites with fewer bandgaps adsorb the maximum fraction of visible light in the spectrum and show increased photocatalytic activity[54]. In the sunlight, there is only 10% UV light for irradiation, much work has been done to use immobilization, non-metal doping with metal oxides, or metal doping with metal oxides to lower the bandgap energy of the resulting nanocomposites to improve the dye degradation. These efforts by Coronado et al. have successfully produced a CeO_2/FAC powered by visible light[55]. The outcomes show that the CeO_2/FAC composite exhibited better-deteriorating performance than pure CeO_2, with its absorption edge shifting into 450 and 800 nm range that is to visible range.

8.0 Conclusion

In present review discussed the development of nanocomposites using various metal/metal oxide nanoparticles coated on cenospheres. Numerous methods, such as energy dispersive X-ray, X-ray diffraction, Fourier Transformation Infrared, ultraviolet-visible spectroscopy, scanning electron microscopy, and transmission electron microscopy, were used to characterize these multiple nanocomposites. All of the nanoparticles' mesoporous shape and the activated fly ash cenosphere's potent adsorption capacity, the combined effect of metals in Al, Na, Ti, S, P, Mg, Fe, K, and Ca then coated metal oxides such as ZnO, V_2O_5, Mn_2O_3, CuO, CeO_2, CdO, Mn_2O_3, metals like Ag and polymer accounted for the notable degradation performance.

9.0 References

1. Chávez-Valdez A, Arizmendi-Morquecho A, Vargas G, Almanza J, Alvarez-Quintana J. Ultra-low thermal conductivity thermal barrier coatings from recycled fly-ash cenospheres. Acta Mater, 2011; 59:2556-62. https://doi.org/10.1016/j.actamat.2011.01.011
2. Ranjbar, N, Kuenzel, C. Influence of preheating of fly ash precursors to produce geopolymers. J Am Ceram Soc. 2017; 100:3165-74. https://doi.org/10.1111/jace.14848
3. Kolay PK, Bhusal S. Recovery of hollow spherical particles with two different densities from coal fly ash and their characterization. Fuel. 2014; 117A:118-24. https://doi.org/10.1016/j.fuel.2013.09.014
4. Blanco F, Garcla P, Mateos P, Ayala J. Characteristics and properties of lightweight concrete manufactured with cenospheres. Cem Concr Res. 2000; 30(11):1715-22. https://doi.org/10.1016/S0008-8846(00)00357-4
5. Gupta N, Woldesenbet E. Microballoon wall thickness effects on properties of syntactic foams. J Cell Plast. 2004; 40(6):461-80. https://doi.org/10.1177/0021955X04048421
6. Drozhzhin VS, Shpirt MY, Danilin LD, Kuvaev MD, Pikulin IV, Potemkin GA, *et al*. Formation processes and main properties of hollow aluminosilicate microspheres in fly ash from thermal power stations. Solid Fuel Chem. 2008; 42:107-19. https://doi.org/10.3103/S0361521908020110
7. Lu Y, Xu S, He M, Chen C, Zhang L, Liu C, *et al*. Glucose administration attenuates spatial memory deficits induced by chronic low-power density microwave exposure. Physiol. Behav. 2012; 106:631-7. https://doi.org/10.1016/j.physbeh.2012.04.019 PMid:22564535
8. Vassilev SV, Menendez R. Phase-mineral and chemical composition of coal fly ashes as a basis for their multicomponent utilization. 4. Characterization of heavy concentrates and improved fly ash residues. Fuel. 2005; 84 (7-8):973-91. https://doi.org/10.1016/j.fuel.2004.11.021
9. Fomenko EV, Anshits NN, Vasilieva NG, Mikhaylova OA, Rogovenko ES, Zhizhaev AM, *et al*. Characterization of fly ash cenospheres produced from the combustion of Ekibastuz coal. Energy Fuels. 2015; 29: 5390-403. https://doi.org/10.1021/acs.energyfuels.5b01022
10. Sokol EV, Volkova NI, Frenkel AE, Maksimova NV, Nigmatulina EN. Hollow silicate microspheres from fly ashes of the Chelyabinsk brown coals (South Urals, Russia). Fuel Process Technol. 2000; 67(1):35-52. https://doi.org/10.1016/S0378-3820(00)00084-9
11. Sarkar A, Rano R, Mishra KK, Mazumder A. Characterization of cenospheres collected from ash-pond of a super thermal power plant, energy sources. Part A: Recovery, utilization, and environmental effects. 2007; 30(3):271-83. https://doi.org/10.1080/00908310600713883

12. Hassan SA, El-Salamony RA. Photocatalytic disc-shaped composite systems for removal of hazardous dyes in aqueous solutions. Can Chem Trans. 2014; 2:57-71. https://doi.org/10.13179/canchemtrans.2014.02.01.0057
13. Holkar CR, Jadhav AJ, Pinjari DV, Mahamuni NM, Pandit AB. A critical review on textile wastewater treatments: Possible approaches. J Environ Manage. 2016; 182:351-66. https://doi.org/10.1016/j.jenvman.2016.07.090 PMid:27497312
14. Neelavannan MG, Basha CA. Electrochemical-assisted photocatalytic degradation of textile wash water. Sep Purif Technol. 2008; 61:168-74. https://doi.org/10.1016/j.seppur.2007.10.009
15. Behnajad MA, Modirshahla N, Hamzavi R. Kinetic study on photocatalytic degradation of C.I. Acid Yellow 23 by ZnO photocatalyst. J Hazard Mater. 2006; 133:226-32. https://doi.org/10.1016/j.jhazmat.2005.10.022 PMid:16310945
16. Das A, Nikhil SK, Nair RG. Influence of surface morphology on the photocatalytic performance of zinc oxide: A review. Nano-Struct Nano-Objects. 2019; 19: 100353. https://doi.org/10.1016/j.nanoso.2019.100353
17. Saravanan R, Gupta VK, Narayanan V, Stephen A. Comparative study on photocatalytic activity of ZnO prepared by different methods. J Mol Liq. 2013; 181: 133-41. https://doi.org/10.1016/j.molliq.2013.02.023
18. He Z, Zhou J. Synthesis, characterization, and activity of tin oxide nanoparticles: Influence of solvothermal time on photocatalytic degradation of rhodamine B. Mod Res Catal. 2013; 2:13. https://doi.org/10.4236/mrc.2013.23A003
19. Anandan K, Rajendran V. Influence of dopant concentrations (Mn=1, 2 and 3mol%) on the structural, magnetic and optical properties and photocatalytic activities of SnO_2 nanoparticles synthesized via the simple precipitation process. Superlattices Microstruct. 2015; 85:185-97. https://doi.org/10.1016/j.spmi.2015.05.031
20. Maciel AP, Longo E, Leite ER. Dióxido de estanho nanoestruturado: Síntese ecrescimento de nanocristais e nanofitas. Química Nova. 2003; 26:855-62. https://doi.org/10.1590/S0100-40422003000600014
21. Chaisitsak S. Nanocrystalline SnO_2: F thin films for liquid petroleum gas sensors. Sensors. 2011; 11:7127. https://doi.org/10.3390/s110707127 PMid:22164007 PMCid:PMC3231694
22. Entradas T, Cabrita JF, Dalui S, Nunes MR, Monteiro OC, Silvestre AJ. Synthesis of sub-5 nm Co-doped SnO_2 nanoparticles and their structural, microstructural, optical and photocatalytic properties. Materials Chemistry and Physics. 2014; 147:563-71. https://doi.org/10.1016/j.matchemphys.2014.05.032
23. Leontie L, Caraman M, Visinoiu A, Rusu GL. On the optical properties of bismuth oxide thin films prepared by pulsed laser deposition. Thin Solid Films. 2005; 473:230-5. https://doi.org/10.1016/j.tsf.2004.07.061
24. Weidong H, Wei Q, Xiaohong W, Xianbo D, Long C, Zhaohua J, The photocatalytic properties of bismuth oxide films prepared through the sol-gel method. Thin Solid Films. 2007; 515:5362-5. https://doi.org/10.1016/j.tsf.2007.01.031
25. Mishra NS, Reddy R, Kuila A, Rani A, Mukherjee P, Nawaz A, *et al.* A review on advanced oxidation processes for effective water treatment. Curr World Environ. 2017; 12(3). ahttps://doi.org/10.12944/CWE.12.3.02
26. Zhang J, Wang B, Cui H, Li C, Zhai J, Li Q. Synthesis of CeO_2/fly ash cenospheres composites as novel photocatalysts by modified pyrolysis process. J Rare Earth. 2014; 32:1120-5. https://doi.org/10.1016/S1002-0721(14)60192-7
27. Hayat K, Gondal MA, Khaled MM, Ahmed S. Effect of operational key parameters on photocatalytic degradation of phenol using nano nickel oxide synthesized by sol-gel method. J Mol Catal A Chem. 2011; 336: 64-71. https://doi.org/10.1016/j.molcata.2010.12.011
28. Lum PT, Foo KY, Zakaria NA, Palaniandy P. Ash-based nanocomposites for photocatalytic degradation of textile dye pollutants: A review. Mater Chem Phys. 2020; 241:122405. https://doi.org/10.1016/j.matchemphys.2019.122405
29. Wang B, Li Q, Wang W, Li Y, Zhai J. Preparation and characterization of Fe^{3+}-doped TiO_2 on fly ash cenospheres for photocatalytic application. Appl Surf Sci. 2011; 257(8):3473-9. https://doi.org/10.1016/j.apsusc.2010.11.050
30. Borges M, Alvarez-Galván M, Esparza P, Medina E, Martín-Zarza P, Fierro J. Ti-containing volcanic ash as photocatalyst for degradation of phenol. Energy Environ Sci. 2008; 1:364-9. https://doi.org/10.1039/b802187m
31. Zhang J, Cui H, Wang B, Li C, Zhai J, Li Q. Fly ash cenospheres supported visible-light-driven $BiVO_4$ photocatalyst: Synthesis, characterization and photocatalytic application. Chem Eng J. 2013; 223:737-46. https://doi.org/10.1016/j.cej.2012.12.065
32. Wu L, Yu J.C, Wang X, Zhang L, Yu J. Characterization of mesoporous nanocrystalline TiO_2 photocatalysts synthesized via a sol-solvothermal process at a low temperature. J Solid State Chem. 2005; 178: 321-8. https://doi.org/10.1016/j.jssc.2004.11.009
33. Adam F, Appaturi JN, Thankappan R, Nawi MAM. Silica-tin nanotubes prepared from rice husk ash by sol-gel method: Characterization and its photocatalytic activity. Appl Surf Sci. 2010; 257:811-16. https://doi.org/10.1016/j.apsusc.2010.07.070
34. Surolia PK, Tayade RJ, Jasra RV. TiO_2-coated cenospheres as catalysts for photocatalytic degradation of methylene blue, p-nitroaniline, n-decane, and n-tridecane under solar irradiation. Ind Eng Chem Res. 2010; 49:8908-19. https://doi.org/10.1021/ie100388m

35. Zhu J, Liu S, Ge J, Guo X, Wang X, Wu H. Synthesis of Fe_2O_3-TiO_2/fly-ash-cenosphere composite and its mechanism of photocatalytic oxidation under visible light. Res Chem Intermed. 2016; 42:3637-54. https://doi.org/10.1007/s11164-015-2236-6
36. Ahmed AE, Adam F. Indium incorporated silica from rice husk and its catalytic activity. Microporous Mesoporous Mater. 2007; 103:284-95. https://doi.org/10.1016/j.micromeso.2007.01.055
37. Endud S, Wong KL. Mesoporous silica MCM-48 molecular sieve modified with $SnCl_2$ in alkaline medium for selective oxidation of alcohol. Microporous Mesoporous Mater. 2007; 101(1-2):256-63. https://doi.org/10.1016/j.micromeso.2006.12.029
38. Wei TY, Kuo CY, Hsu YJ, Lu SY, Chang YC. Tin oxide nanocrystals embedded in silica aerogel: Photoluminescence and photocatalysis. Microporous Mesoporous Mater. 2008; 112:580-8. https://doi.org/10.1016/j.micromeso.2007.10.040
39. Wang B, Yang Z, An H, Zhai J, Li Q, Cui H. Photocatalytic activity of Pt-TiO_2 films supported on hydroxylated fly ash cenospheres under visible light. Appl Surf Sci. 2015; 324:817-24. https://doi.org/10.1016/j.apsusc.2014.11.046
40. Thejaswini TVL, Prabhakaran D, Maheswari MA. Soft synthesis of Bi-Doped and Bi-N co-doped TiO_2 nanocomposites: A comprehensive mechanistic approach towards visible light-induced ultra-fast photocatalytic degradation of fabric dye pollutant. J Environ Chem Eng. 2016; 4:1308-21. https://doi.org/10.1016/j.jece.2016.01.031
41. Chandra MR, Rao TS, Pammi SVN, Sreedhar B. An enhanced visible light active rutile titania-copper/polythiophene nanohybrid material for the degradation of rhodamine B dye. Mater Sci Semicond Process. 2015; 30:672-81. https://doi.org/10.1016/j.mssp.2014.09.009
42. Li SQ, Zhou PJ, Zhang WS, Chen S, Peng H. Effective photocatalytic decolorization of methylene blue utilizing ZnO/rectorite nanocomposite under simulated solar irradiation. J Alloys Compd. 2014; 616:227-34. https://doi.org/10.1016/j.jallcom.2014.07.102
43. Sangami G, Dharmaraj N. UV-visible spectroscopic estimation of photodegradation of rhodamine-B dye using tin(IV) oxide nanoparticles. Spectrochim. Acta A Mol. Biomol. Spectrosc. 2012; 97:847-52. https://doi.org/10.1016/j.saa.2012.07.068 PMid:22902583
44. Ameta N, Sharma J, Sharma S, Kumar S, Punjabi PB. Copper modified iron oxide as heterogeneous photo-Fenton reagent for the degradation of coomasie Brilliant Blue R-250. Indian J Chem. 2012; 51A:943-8.
45. Sudha G, Subramanian E, Murugan C. Development of iron oxide/zeo-NaX nano photocatalyst from coal fly ash and its activity assessment by methylene blue dye degradation. Int J Natu Appl Sci. 2015; 2:114-28. https://doi.org/10.1016/j.materresbull.2013.12.006
46. Ren C, Yang B, Wu M, Xu J, Fu Z, lv Y, *et al*. Synthesis of Ag/ZnO nanorods array with enhanced photocatalytic performance. J Hazard Mater. 2010; 182:123-9. https://doi.org/10.1016/j.jhazmat.2010.05.141 PMid:20580489
47. Ahmed S, Rasul MG, Martens WN, Brown R, Hashib MA. Heterogeneous photocatalytic degradation of phenols in wastewater: A review on current status and developments. Desalination. 2010; 261:3-18. https://doi.org/10.1016/j.desal.2010.04.062
48. Gupta VK, Jain R, Mittal A, Saleh TA, Nayak A, Agarwal S, *et al*. Photo-catalytic degradation of toxic dye amaranth on TiO_2/UV in aqueous suspensions. Mater Sci Eng C. 2012; 32:12-17. https://doi.org/10.1016/j.msec.2011.08.018 PMid:23177765
49. Soltani RDC, Khataee A, Mashayekhi M. Photocatalytic degradation of a textile dye in aqueous phase over ZnO nanoparticles embedded in biosilica nanobiostructure. Desalin Water Treat. 2016; 57:13494-504. https://doi.org/10.1080/19443994.2015.1058193
50. Subash B, Krishnakumar B, Sreedhar B, Swaminathan M, Shanthi M. Highly active WO_3-Ag-ZnO photocatalyst driven by daylight illumination. Superlattices Microstruct. 2013; 54:155-71. https://doi.org/10.1016/j.spmi.2012.11.009
51. Uddin MT, Sultana Y, Islam MA. Nano-sized SnO_2 photocatalysts: synthesis, characterization and their application for the degradation of Methylene Blue dye. J Sci Res. 2016; 8:399-411. https://doi.org/10.3329/jsr.v8i3.27524
52. Peng X, Luan Z, Ding J, Di Z, Li Y, Tian B. Ceria nanoparticles supported on carbon nanotubes for the removal of arsenate from water. Mater Lett. 2005; 59:399-403. https://doi.org/10.1016/j.matlet.2004.05.090
53. Kalpana K, Selvaraj V. Photodegradation and antibacterial studies of ZnS enwrapped fly ash nanocomposite for multipurpose industrial applications. RSC Adv. 2015; 5:47766-77. https://doi.org/10.1039/C4RA16642F
54. Saravanan R, Gracia F, Stephen A. Basic principles, mechanism, and challenges of photocatalysis. Nanocomposites for visible light-induced photocatalysis. Springer; 2017. p. 19-40. https://doi.org/10.1007/978-3-319-62446-4_2
55. Coronado JM, Fresno F, Hernández-Alonso MD, Portela R. Design of advanced photocatalytic materials for energy and environmental applications. Springer, 2013. https://doi.org/10.1007/978-1-4471-5061-9